JOURNAL OF POLYMER SCIENCE | PART B

Polymer Physics

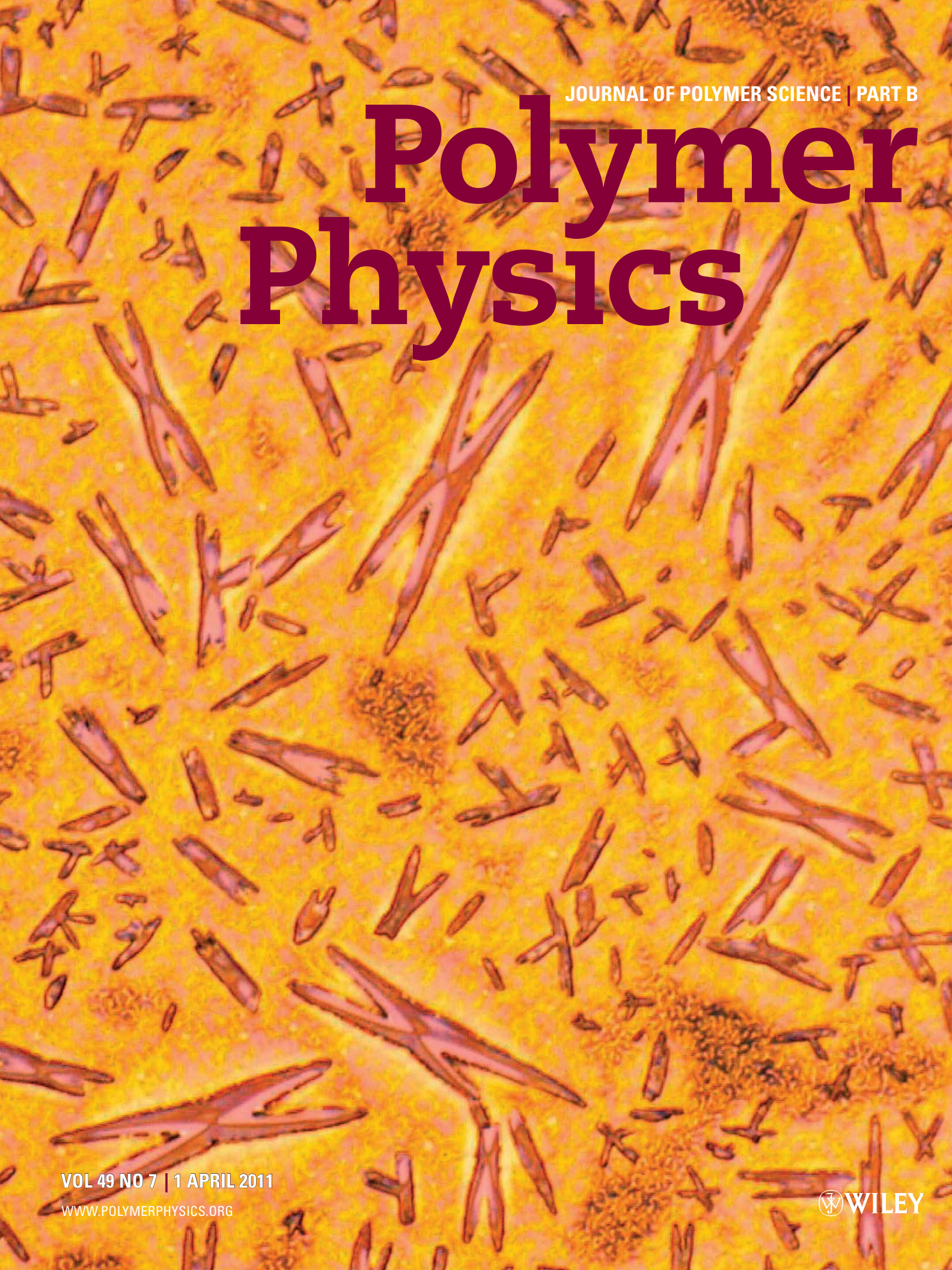

VOL 49 NO 7 | 1 APRIL 2011
WWW.POLYMERPHYSICS.ORG

WILEY

Polymer Physics

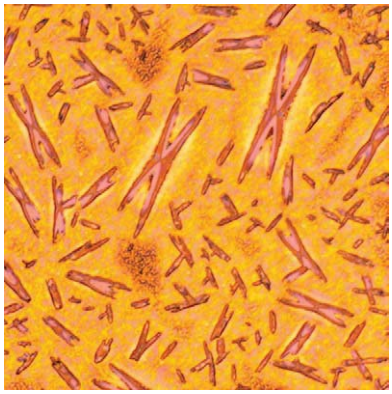

POLYMER SOLAR CELLS

Polymer solar cells are a low-cost alternative to inorganic photovoltaics, but reaching commercially viable efficiencies is heavily dependent on understanding and control of the polymer blend morphology in the devices, no matter which polymer is used. On page 499 of this issue, Nichole Cates Miller and colleagues construct the eutectic phase diagram of blends of the polymer pBTTT and fullerene derivative $PC_{71}BM$. The phase diagram explains why solar cells with 75-80 wt % fullerene perform best, since these blends have both electron- and hole-conducting phases at room temperature, ensuring clear charge-conduction pathways to the electrodes. In addition, the authors also show how to suppress intercalation of the fullerene between the polymer side chains using rapid thermal annealing. The cover is an optical microscopy image of the phase separation in a 1:1 pBTTT:$PC_{71}BM$ blend that has been annealed above the eutectic temperature.

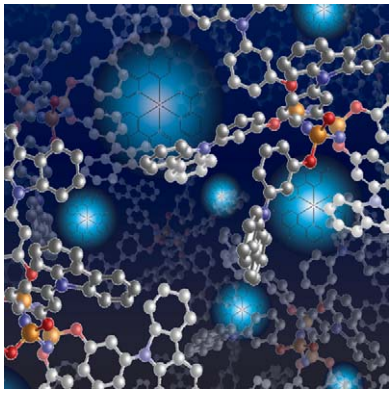

DENDRIMERS

Dendrimers have several advantages over polymers for electronics, including separate control of the surface groups and the core, which allows the processing and optoelectronic properties to be changed independently. They can be used as host materials for phosphorescent light-emitting diodes, where energy is transferred to emissive guest molecules. Efficient materials with solution processability, sufficient thermal properties and wide bandgaps capable of transferring energy to blue-light-emitting guests have been elusive. On page 531 of this issue, Alan Sellinger and colleagues report solution-processable high bandgap hosts with carbazole-functionalized cyclic phosphazene cores. The materials are amorphous with high glass transition temperatures due to their 3D rigid architecture, which simplifies processing. In addition, the optical and electronic properties depend solely on the dendrons, which can be selected to produce highly efficient devices with blue through to red emission. Inside cover art by Dr. Zien Ooi.

Coming soon Look for these important papers in upcoming issues of Polymer Physics

Keith C. Gallow, Young K. Jhon, Wei Tang, Jan Genzer, and Yueh-Lin Loo
Cloud Point Suppression in Dilute Solutions of Model Gradient Copolymers with Pre-specified Composition Profiles
DOI: 10.1002/polb.22226

Dinesh G. "Dan" Patel, Yu-ya Ohnishi, Yixing Yang, Sang-Hyun Eom, Richard T. Farley, Kenneth R. Graham, Jiangeng Xue, So Hirata, Kirk S. Schanze, and John R. Reynolds
Conjugated Polymers for Pure UV Light Emission: Poly(*meta*-phenylenes)
DOI: 10.1002/polb.22224

Oguz Okay
DNA Hydrogels: New Functional Soft Materials
DOI: 10.1002/polb.22213

All our articles are available online in advance of print. The articles listed here have been judged by either the referees or the editor to be very important, and were immediately copyedited, proofread and published online. As long as there is no page number available, online manuscripts should be cited in the following manner: Authors, *J. Polym. Sci. Part B: Polym. Phys.*, online publication date, DOI

The Phase Behavior of a Polymer-Fullerene Bulk Heterojunction System that Contains Bimolecular Crystals

Nichole Cates Miller,[1] Roman Gysel,[1] Chad E. Miller,[1,2] Eric Verploegen,[2,3] Zach Beiley,[1] Martin Heeney,[4] Iain McCulloch,[4] Zhenan Bao,[3] Michael F. Toney,[2] Michael D. McGehee[1]

[1]Department of Materials Science and Engineering, Stanford University, Stanford, California 94305

[2]Stanford Synchrotron Radiation Lightsource, SLAC National Accelerator Laboratory, Menlo Park, California 94025

[3]Department of Chemical Engineering, Stanford University, Stanford, California 94305

[4]Department of Chemistry, Imperial College, London SW7 2AZ, United Kingdom

Correspondence to: M. D. McGehee (E-mail: mmcgehee@stanford.edu)

Received 10 December 2010; revised 23 January 2011; accepted 26 January 2011; published online 2011
DOI: 10.1002/polb.22214

ABSTRACT: Polymer:fullerene blends have been widely studied as an inexpensive alternative to traditional silicon solar cells. Some polymer:fullerene blends, such as blends of poly(2,5-bis(3-tetradecylthiophen-2-yl)thieno[3,2-b]thiophene (pBTTT) with phenyl-c71-butyric acid methyl ester ($PC_{71}BM$), form bimolecular crystals due to fullerene intercalation between the polymer side chains. Here we present the determination of the eutectic pBTTT:$PC_{71}BM$ phase diagram using differential scanning calorimetry (DSC) and two-dimensional grazing incidence X-ray scattering (2D GIXS) with in-situ thermal annealing. The phase diagram explains why the most efficient pBTTT:$PC_{71}BM$ solar cells have 75–80 wt % $PC_{71}BM$ since these blends lie in the center of the only room-temperature phase region containing both electron-conducting ($PC_{71}BM$) and hole-conducting (bimolecular crystal) phases. We show that intercalation can be suppressed in 50:50 pBTTT:$PC_{71}BM$ blends by using rapid thermal annealing to heat the blends above the eutectic temperature, which forces $PC_{71}BM$ out of the bimolecular crystal, followed by quick cooling to kinetically trap the pure $PC_{71}BM$ phase. © 2011 Wiley Periodicals, Inc. J Polym Sci Part B: Polym Phys 49: 499–503, 2011

KEYWORDS: conjugated polymers; differential scanning calorimetry (DSC); phase diagrams; X-ray

INTRODUCTION Polymer:fullerene bulk heterojunction (BHJ) solar cells show promise as a low-cost, printable, and flexible sustainable energy source.[1–5] BHJ solar cells, which have achieved power conversion efficiencies in excess of 8%,[6–9] consist of an interpenetrating network of an electron-donating conjugated polymer and an electron-accepting fullerene derivative. The composition and annealing conditions can drastically affect solar-cell performance, demonstrating the importance of understanding the phase behavior of polymer:fullerene blends.[10–13]

Phase diagrams have proven to be useful tools for understanding material properties as a function of composition and temperature for both inorganic[14,15] and organic[13,16,17] mixtures. Polymer:fullerene phase diagrams have improved understanding of BHJ optimal compositions,[13] annealing conditions,[16] and charge transport properties.[17] To date, no one has determined the phase diagram of a polymer:fullerene blend that forms bimolecular crystals due to fullerene intercalation between the polymer side chains.[10] Intercalation affects solar-cell performance[10,11] and charge transport[10,18] and is likely to influence the phase diagram.

Here, we present the determination and importance of the phase diagram of a polymer:fullerene blend that can form bimolecular crystals. We study blends of poly(2,5-bis(3-tetradecylthiophen-2-yl)thieno[3,2-b]thiophene (pBTTT) with phenyl-c71-butyric acid methyl ester ($PC_{71}BM$), since $PC_{71}BM$ molecules are known to intercalate between the pBTTT side chains to form a pBTTT:$PC_{71}BM$ bimolecular crystal.[10,11,19,20] The structures of pBTTT and $PC_{71}BM$ are shown in Figure 1. pBTTT is a conjugated polymer used in organic transistors because of its exceptionally high mobility parallel to the substrate,[21] and pBTTT:$PC_{71}BM$ blends have been used as the active layer in some BHJ solar cells.[22,23] Here, we show how intercalation affects the pBTTT:$PC_{71}BM$ phase diagram and how thermal treatments inspired by the phase diagram can suppress intercalation.

RESULTS AND DISCUSSION

Differential scanning calorimetry (DSC) was used to determine the transition temperatures of pBTTT:$PC_{71}BM$ blends at a variety of compositions. Figure 2 shows key DSC scans and the eutectic phase diagram produced by plotting the

Additional Supporting Information may be found in the online version of this article.

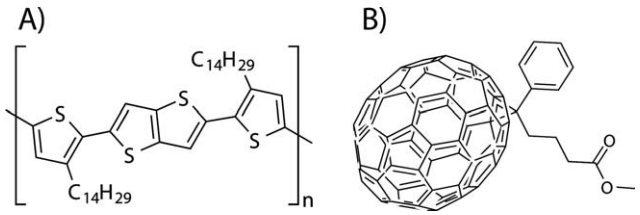

FIGURE 1 Chemical structures of (A) pBTTT and (B) $PC_{71}BM$.

transitions on a temperature-concentration plot. Two-dimensional grazing incidence X-ray scattering (2D GIXS) with in-situ thermal annealing[24] was used to verify the phases present in each region of the phase diagram (Fig. 3). The phase diagram was further validated by the agreement between measured enthalpies for $PC_{71}BM$ melting in the hypereutectic mixtures and enthalpies calculated by scaling the melting enthalpy of pure $PC_{71}BM$ by the weight fraction of the pure $PC_{71}BM$ phase at the $PC_{71}BM$ melting temperature (see Supporting Information).

DSC of pure pBTTT shows phase transitions at ~137 and ~232 °C; these transitions have been attributed to side-chain melting (the formation of a liquid crystalline phase) and complete polymer melting, respectively (Fig. 2).[21,25] The 2D GIXS pattern of the solid polymer at 25 °C [Fig. 3(A)] shows a lamellar structure with a spacing of ~21 Å. Thus, we use a lamellar spacing of ~21 Å to identify pure pBTTT. Upon heating to 180 °C, the polymer, which is liquid crystalline at this temperature, exhibits increased angular alignment out of the plane of the substrate, as indicated by the decreased arcing of the peaks [Fig. 3(B)]. Heating to 250 °C causes the diffraction peaks to disappear and be replaced by a broad ring from the liquid polymer [Fig. 3(C)].

DSC of pure $PC_{71}BM$ shows an exothermic peak due to crystallization at ~204 °C and a melting peak at ~319 °C (Fig. 2). The $PC_{71}BM$ crystallization peak is marked with a red x on the phase diagram. At 25 °C the 2D GIXS pattern shows only a broad ring [Fig. 3(M)], indicating that the $PC_{71}BM$ is amorphous; amorphous $PC_{71}BM$ is expected at room temperature since the DSC data shows that pure $PC_{71}BM$ does not crystallize below ~204 °C. Heating the $PC_{71}BM$ above the crystallization temperature to 250 °C causes the formation of randomly oriented large $PC_{71}BM$ crystallites as illustrated by the sharp diffraction rings in Figure 3(N).

The pure pBTTT:$PC_{71}BM$ bimolecular crystal occurs at a 40:60 polymer:fullerene weight ratio, which is equivalent to a 1:1 monomer:fullerene molar ratio.[20] Since the bimolecular crystal has a well-defined polymer:fullerene ratio, we have included the bimolecular crystal on the phase diagram as a line compound at 60 wt % $PC_{71}BM$, although in reality there may be some phase-field width. The DSC curve for the 40:60 blend shows transitions at ~225 °C (the eutectic temperature) and ~319 °C (the $PC_{71}BM$ melting temperature) [Fig. 2(A)]. It is not surprising that no side-chain melting peak (~137 °C) is observed for the bimolecular crystal, since it has largely disordered side chains at room temperature.[20] The bimolecular crystal has a lamellar structure with a spacing of ~30 Å [Fig 3(G,H)].[10,20] The pi-stacking distance of the bimolecular crystal is the same as the pi-stacking distance of pure pBTTT.[20] Like the pure polymer, the bimolecular crystal shows increased out-of-plane alignment upon heating to 180 °C. At 250 °C, which is above the eutectic temperature, the 40:60 pBTTT:$PC_{71}BM$ blend exhibits two phases: crystalline $PC_{71}BM$ (sharp rings) and a liquid phase (broad ring) that contains both pBTTT and $PC_{71}BM$ [Fig. 3(I)].

Below the eutectic temperature, the polymer-rich 80:20 pBTTT:$PC_{71}BM$ blend consists of pure pBTTT and the bimolecular crystal, as indicated by the coexistence of lamellar structures with spacings of ~21 Å and ~30 Å [Fig. 3(D,E) and Supporting Information].[10] The DSC measurements show a weak peak at ~137 °C due to side-chain melting. Since side-chain melting only occurs in the pure polymer, solid pBTTT coexists with the bimolecular crystal below the side-

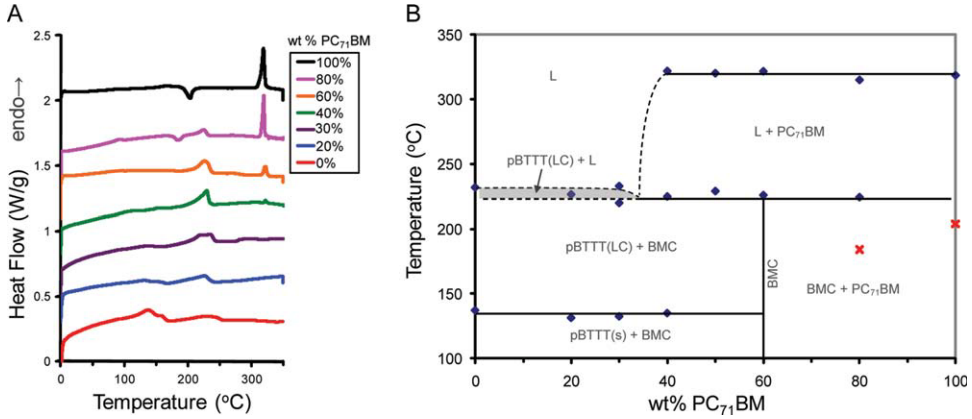

FIGURE 2 (A) Key DSC curves for the second heating of the pBTTT:$PC_{71}BM$ blends. (B) The pBTTT:$PC_{71}BM$ phase diagram with the peak positions from the DSC scans marked with blue diamonds and the $PC_{71}BM$ crystallization peak positions marked with red x's. L, LC, s, and BMC stand for liquid, liquid crystal, solid, and bimolecular crystal, respectively.

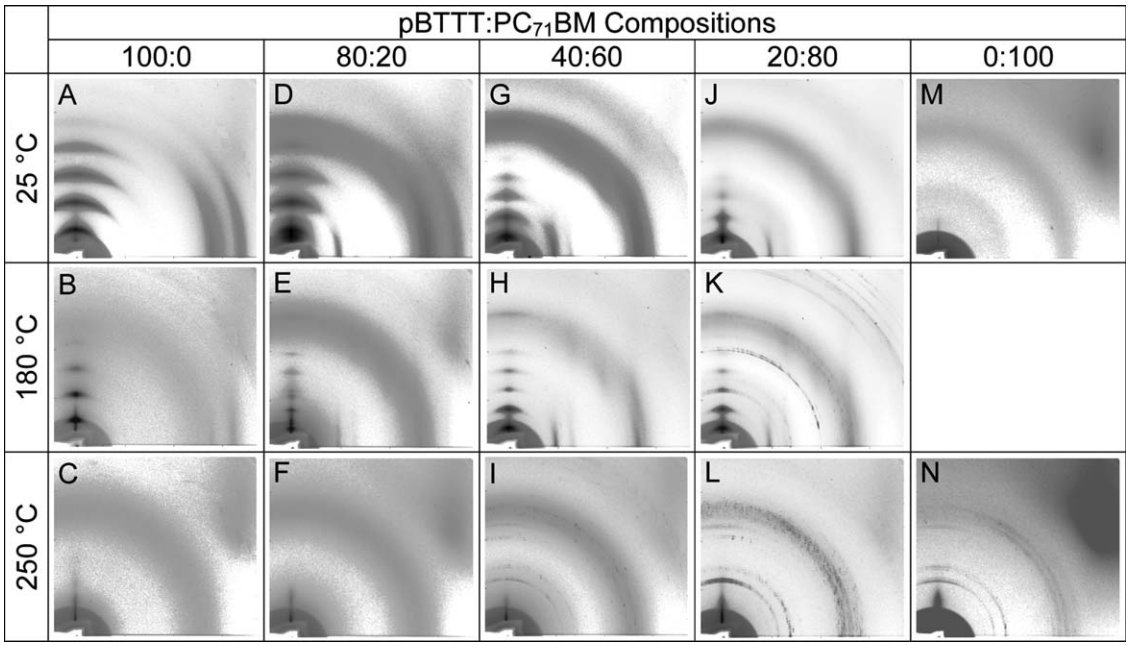

FIGURE 3 2D GIXS patterns for pBTTT:$PC_{71}BM$ blends at a variety of compositions and temperatures. Each image shows q_z from 0 to 1.9 $Å^{-1}$ on the vertical axis and q_{xy} from −0.2 to 1.9 $Å^{-1}$ on the horizontal axis.

chain melting temperature (∼137 °C), and liquid crystalline pBTTT coexists with the bimolecular crystal between the side-chain melting temperature and the eutectic temperature (∼225 °C). Only the liquid phase is observed at 250 °C [Fig. 3(F)]. There is some uncertainty in the transition temperatures described by the dashed lines in the phase diagram [Fig. 2(B)] due to the close proximity of the polymer melting temperature (∼232 °C) to the eutectic temperature (∼225 °C) and the resulting difficulty in differentiating the two transitions in the DSC scans and in performing 2D GIXS experiments in such a small temperature range. We are, however, confident that the phase diagram is eutectic due to the agreement of the observed scaling of the $PC_{71}BM$ melting enthalpies with those estimated assuming a eutectic phase diagram with a eutectic composition of 35 wt % $PC_{71}BM$ (see Supporting Information), the presence of a small $PC_{71}BM$ melting peak in blends with 40 wt % $PC_{71}BM$ and this peak's absence in blends with only 30 wt % $PC_{71}BM$, and the thermodynamic requirement for a binary mixture in a phase region bounded by two pure phases [liquid and pure liquid-crystalline pBTTT in the case of the shaded region in Fig. 2(B)] to minimize its Gibb's free energy by forming a mixture of the two bounding phases.

The 2D GIXS pattern of the fullerene-rich 20:80 pBTTT:$PC_{71}BM$ blend shows a lamellar structure with a spacing of ∼30 Å (the bimolecular crystal) and an amorphous ring ($PC_{71}BM$) at room temperature [Fig. 3(J)]. DSC of this blend shows an exothermic $PC_{71}BM$ crystallization peak at ∼182 °C (Fig. 2), so it is not surprising that the $PC_{71}BM$ is crystalline in the 2D GIXS pattern of the blend at 180 °C [Fig. 3(K)]. The depression of the $PC_{71}BM$ crystallization temperature in the 20:80 pBTTT:$PC_{71}BM$ blend (∼182 °C) relative to pure $PC_{71}BM$ (∼204 °C) is similar to the $PC_{61}BM$ crystallization temperature depression observed in P3HT:$PC_{61}BM$ blends.[24] Heating the 20:80 blend to 250 °C causes the lamellar structure to disappear while the $PC_{71}BM$ diffraction rings remain, indicating the coexistence of a liquid phase with crystalline $PC_{71}BM$ [Fig. 3(L)].

The 20:80 pBTTT:$PC_{71}BM$ blend is the only blend shown in Figure 3 that at room temperature contains both electron- and hole-conducting phases, which are needed for efficient charge extraction and good solar-cell performance. It is therefore not surprising that the optimal composition for pBTTT:$PC_{71}BM$ solar cells is 75–80 wt % $PC_{71}BM$.[10,18,22,23] Müller et al. demonstrated that several poly(3-alkylthiophene):fullerene solar cells exhibited optimal performance at slightly hypereutectic compositions when the composition is expressed in terms of the fullerene concentration, since slightly hypereutectic blends have both fine phase separation and balanced charge transport.[13] This model is remarkably accurate at predicting the optimal compositions of poly(3-alkylthiophene):fullerene blends, which do not contain bimolecular crystals. Intercalation complicates matters, since blends with intercalation may have very little, if any, electron-conducting phase (pure fullerene) at slightly hypereutectic compositions. For instance, slightly hypereutectic pBTTT:$PC_{71}BM$ blends, which have ∼50 wt % $PC_{71}BM$ since the eutectic composition is ∼35 wt % $PC_{71}BM$, exhibit inefficient electron extraction and poor solar-cell performance because only hole-conducting phases (pure pBTTT and the bimolecular crystal) exist at room temperature.[10,11]

The pBTTT:$PC_{71}BM$ phase diagram reveals that an electron-conducting, pure $PC_{71}BM$ phase coexists with a liquid phase

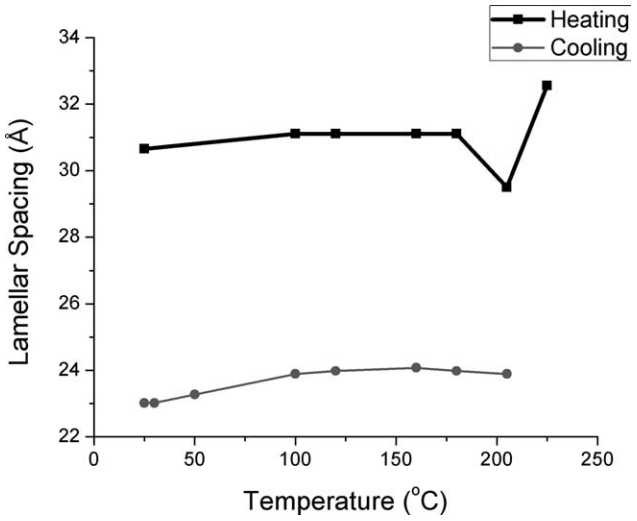

FIGURE 4 Lamellar spacings, measured using specular diffraction with in-situ temperature annealing, as a function of temperature for a 50:50 pBTTT:$PC_{71}BM$ blend during heating (black) and cooling (gray). The blend was heated to 275 °C, but no peaks could be observed at temperatures above 225 °C.

in blends with ~50 wt % $PC_{71}BM$ at temperatures above the eutectic temperature (~225 °C). If the pure $PC_{71}BM$ phase could be preserved upon cooling, an efficient 50:50 pBTTT:$PC_{71}BM$ solar cell might be possible since the film would have both electron- and hole-conducting phases. Using specular X-ray diffraction with in-situ annealing, we show that heating a 50:50 pBTTT:$PC_{71}BM$ blend above the eutectic temperature and then cooling it to room temperature causes the lamellar spacing to decrease from ~30 to ~23 Å (Fig. 4). The temperature dependence of the lamellar spacings of the bimolecular crystal during heating and the pure polymer during cooling can be attributed to thermal expansion and side-chain melting.[25] The relatively fast cooling rates used in these experiments results in the formation of nearly pure pBTTT and $PC_{71}BM$ rather than the bimolecular crystal upon cooling from above the eutectic temperature. Significantly slower cooling should result in the formation of the bimolecular crystal, since the thermal stability of the bimolecular crystal was previously verified by the formation of the bimolecular crystal upon annealing of nonintercalated pBTTT:$PC_{71}BM$ bilayer films at temperatures below the eutectic temperature.[20]

Although quick cooling from above the eutectic temperature results in the formation of an electron-conducting $PC_{71}BM$ phase, extended periods of time spent above the eutectic temperature are likely to result in phase separated domains that are significantly larger than the exciton diffusion length in polymers, thus causing poor solar-cell performance. We therefore attempted to quickly heat the samples above the eutectic temperature using rapid thermal annealing (RTA) followed by fast cooling in order to cause the $PC_{71}BM$ to phase separate from the bimolecular crystal without giving enough time for large-scale phase separation to occur. RTA is used extensively in the inorganic electronics community,[26,27] but has yet to be widely adopted by the organic electronics community. RTA heats the film from the top using a flash lamp and then quickly cools the sample by conduction through a metal plate. Although we were able to control intercalation using RTA (see Supporting Information), we have not yet been able to make efficient solar cells using this method. One problem is that the solar cells are exposed to oxygen before and after the RTA process since this setup is not enclosed in a glovebox. In addition, the samples for which intercalation was suppressed exhibit micron-scale phase separation, which is not desirable in BHJ solar cells. We do, however, believe that RTA shows promise as method to manipulate the phases in polymer:fullerene blends.

CONCLUSIONS

The pBTTT:$PC_{71}BM$ phase diagram was constructed using a combination of DSC and temperature-dependent 2D GIXS. The phase diagram explains why pBTTT:$PC_{71}BM$ solar cells with 75–80 wt % $PC_{71}BM$ perform best since these blends have both electron- and hole-conducting phases at room temperature. We demonstrate the ability to process pure pBTTT and pure $PC_{71}BM$ phases rather than the thermodynamically favorable bimolecular crystal in blends with 50 wt % $PC_{71}BM$ by cooling the blends quickly from above the eutectic temperature. We also show that RTA can be used to suppress intercalation in pBTTT:$PC_{71}BM$ blends.

EXPERIMENTAL

Materials

pBTTT was synthesized with C14 side chains as described in ref. 21, and $PC_{71}BM$ was purchased from NanoC. The pBTTT had a number average molecular mass (M_n) of 22 KDa with a polydispersity of 2.0, as determined by gel permeation chromatography against polystyrene standards.

Differential Scanning Calorimetry (DSC)

Samples for DSC were prepared by dissolving pBTTT and $PC_{71}BM$ in ortho-dichlorobenzene (DCB) and drop casting the solutions onto clean glass substrates. The dried films were scraped off the substrates with a razor blade and placed in hermetically sealed pans. The samples were measured in flowing nitrogen using a TA Instruments Q100 DSC with heating and cooling rates of 10 °C/min. The first run only heated the samples to 170 °C, because heating the blends above ~225 °C and cooling at a rate of 10 °C/min results in incomplete intercalation for the second run due to kinetically trapped pure pBTTT and pure $PC_{71}BM$ phases (see Supporting Information).

X-Ray Diffraction

Samples for X-ray diffraction were prepared by spin coating pBTTT:$PC_{71}BM$ blends from a DCB solution onto octadecyltrichlorosilane (OTS)-coated silicon substrates. OTS increases the crystalline order, making the weaker diffraction peaks easier to detect, but does not change the peak positions.[11] 2D GIXS measurements were performed at the Stanford Synchrotron Radiation Lightsource (SSRL) on beamline 11-3

using a MAR345 image plate area detector. The 2D GIXS measurements were carried out at an energy of 12.7 keV and an incidence angle of 0.10 degrees. For the in-situ heating measurements, there is a 3 °C uncertainty in the film temperature due to temperature variations as a function of time and position on the film. Additional details on the in-situ heating measurements can be found elsewhere (ref. 22). Specular diffraction was performed on SSRL beamline 2-1 at an energy of 8 keV. An Anton-Parr DSC 9000 furnace was used for the annealing studies on this beamline.

Rapid Thermal Annealing (RTA)

Samples were heated under flowing nitrogen in a AG Associates Heatpulse 210 Rapid Thermal Annealer. The samples reached 270 °C within 10 sec and were kept at this temperature for 5, 10, and 20 sec before cooling. The samples were exposed to air for ~50 min at room temperature.

ACKNOWLEDGMENTS

The authors would like to acknowledge the use of the diffraction-image-processing and data-analysis software package WxDiff by Stefan C.B. Mannsfeld, SSRL (http://code.google.com/p/wxdiff). This work was supported by the Department of Energy, Office of Basic Energy Sciences, Division of Materials Sciences and Engineering, under contract DE-AC02-76SF00515. Nichole Miller, Roman Gysel, Eric Verploegen, and Zach Beiley were also supported by a National Science Foundation Graduate Research Fellowship, a Swiss National Science Foundation Postdoctoral Fellowship, a Fellowship from Eastman Kodak Corporation, and a National Defense Science and Engineering Graduate Fellowship, respectively. Portions of this research were carried out at the Stanford Synchrotron Radiation Lightsource (SSRL), a national user facility operated by Stanford University on behalf of the US Department of Energy, Office of Basic Energy Sciences.

REFERENCES AND NOTES

1 Dennler, G.; Scharber, M. C.; Brabec, C. J. *Adv. Mater.* **2009,** *21*, 1323–1338.

2 Thompson, B. C.; Frechet, J. M. J. *Angew. Chem. Int. Ed.* **2008,** *47*, 58–77.

3 Mayer, A. C.; Scully, S. R.; Hardin, B. E.; Rowell, M. W.; McGehee, M. D. *Mater. Today* **2007,** 28–33.

4 Blom, P. W. M.; Mihailetchi, V. D.; Koster, L. J. A.; Markov, D. E. *Adv. Mater.* **2007,** *19*, 1551–1566.

5 Kippelen, B.; Brédas, J.-L. *Energy Environ. Sci.* **2009,** 251–261.

6 Park, S. H.; Roy, A.; Beaupre, S.; Cho, S.; Coates, N.; Moon, J. S.; Moses, D.; Leclerc, M.; Lee, K.; Heeger, A. J. *Nat. Photonics* **2009,** *3*, 297–302.

7 Liang, Y.; Xu, Z.; Xia, J.; Tsai, S. T.; Wu, Y.; Li, G.; Ray, C.; Yu, L. *Adv. Mater.* **2010,** *22*, E135–E138.

8 Solarmer Energy, Inc. Breaks Psychological Barrier with 8.13% OPV Efficiency; July 27, **2010.**

9 Konarka's Power Plastic Achieves World Record 8.3% Efficiency Certification from National Energy Renewable Laboratory (NREL); November 29, **2010.**

10 Mayer, A. C.; Toney, M. F.; Scully, S. R.; Rivnay, J.; Brabec, C. J.; Scharber, M.; Koppe, M.; Heeney, M.; McCulloch, I.; McGehee, M. D. *Adv. Funct. Mater.* **2009,** *19*, 1173–1179.

11 Cates, N. C.; Gysel, R.; Beiley, Z.; Miller, C. E.; Toney, M. F.; Heeney, M.; McCulloch, I.; McGehee, M. D. *Nano. Lett.* **2009,** *9*, 4153–4157.

12 Ma, W., Yang, C., Gong, X., Lee, K., Heeger, A. J. *Adv. Func. Mater.* **2005,** *15*, 1617–1622.

13 Müller, C.; Ferenczi, T. A. M.; Campoy-Quiles, M.; Frost, J. M.; Bradley, D. D. C.; Smith, P.; Stingelin-Stutzmann, N.; Nelson, J. *Adv. Mater.* **2008,** *20*, 3510–3515.

14 Korkishko, Y. N.; Fedorov, V. A. *IEEE J. Sel. Top Quantum Electron* **1996,** *2*, 187–196.

15 Matijasevic, G. S.; Lee, C. C.; Wang, C. Y. *Thin Solid Films* **1993,** *223*, 276–287.

16 Zhao, J.; Swinnen, A.; Van Assche, G.; Manca, J.; Vanderzande, D.; Mele, B. V. *J. Phys. Chem. B* **2009,** *113*, 1587–1591.

17 Kim, J. Y.; Frisbie, C. D. *J. Phys. Chem. C* **2008,** *112*, 17726–17736.

18 Cates, N. C.; Gysel, R.; Dahl, J. E. P.; Sellinger, A.; McGehee, M. D. *Chem. Mater.* **2010,** *22*, 3543–3548.

19 Savenije, T. J.; Grzegorczyk, W. J.; Heeney, M.; Tierney, S.; McCulloch, I.; Siebbeles, L. D. A. *J. Phys. Chem. C 114*, 15116–15120.

20 Gysel, R.; Cho, E.; Miller, N. C.; Risko, C.; Kim, D.; Miller, C. E.; Richter, L.; Kline, R. J.; Heeney, M.; McCulloch, I.; Toney, M. F.; Brédas, J.-L.; McGehee, M. D., submitted for publication.

21 McCulloch, I.; Heeney, M.; Bailey, C.; Genevicius, K.; Macdonald, I.; Shkunov, M.; Sparrowe, D.; Tierney, S.; Wagner, R.; Zhang, W. M.; Chabinyc, M. L.; Kline, R. J.; McGehee, M. D.; Toney, M. F. *Nat. Mater.* **2006,** *5*, 328–333.

22 Parmer, J. E.; Mayer, A. C.; Hardin, B. E.; Scully, S. R.; McGehee, M. D.; Heeney, M.; McCulloch, I. *Appl. Phys. Lett.* **2008,** *92*, 113309.

23 Hwang, I.-W.; Young Kim, J.; Cho, S.; Yuen, J.; Coates, N.; Lee, K.; Heeney, M.; McCulloch, I.; Moses, D.; Heeger, A. J. *J. Phys. Chem. C* **2008,** *112*, 7853–7857.

24 Verploegen, E.; Mondal, R.; Bettinger, C. J.; Sok, S.; Toney, M. F.; Bao, Z. *Adv. Funct. Mater.* **2010,** *20*, 3519–3529.

25 DeLongchamp, D. M.; Kline, R. J.; Jung, Y.; Lin, E. K.; Fischer, D. A.; Gundlach, D. J.; Cotts, S. K.; Moad, A. J.; Richter, L. J.; Toney, M. F.; Heeney, M.; McCulloch, I. *Macromolecules* **2008,** *41*, 5709–5715.

26 Liu, G.; Fonash, S. J. *Appl. Phys. Lett.* **1989,** *55*, 660–662.

27 Xu, S. J.; Wang, X. C.; Chua, S. J.; Wang, C. H.; Fan, W. J.; Jiang, J.; Xie, X. G. *Appl. Phys. Lett.* **1998,** *72*, 3335–3337.